Environ. Sci. Technol. **1997**, *31,* 2005−2011

Adsorption and Stability of Arsenic(III) at the Clay Mineral−Water Interface

BRUCE A. MANNING* AND SABINE GOLDBERG
USDA-ARS U.S. Salinity Laboratory, 450 West Big Springs Road, Riverside, California 92507-4617

Adsorption and oxidation reactions of arsenite (As(III)) at the mineral−water interface are two important factors affecting the fate and transport of arsenic in the environment. Numerous studies have concluded that As(III) is more soluble and mobile than arsenate (As(V)) in soils, though very little experimental work has demonstrated the differences in reactivity and stability of As(III) and As(V) at the mineral−water interface. In this investigation, As(III) adsorption on kaolinite, illite, montmorillonite, and amorphous aluminum hydroxide (am-Al$(OH)_3$) was studied as a function of pH and ionic strength and was compared with As(V) adsorption. High-performance liquid chromatography−hydride generation atomic absorption spectrophotometry (HPLC−HGAAS) was employed for direct determination of As(III) and As(V). In addition, surface complexation modeling was used to describe As(III) and As(V) adsorption on the four minerals. It was revealed that alkaline solutions (pH > 9) without mineral solids caused homogeneous oxidation of As(III) to As(V). In addition, recovery of adsorbed As from As(III)-treated clay mineral solids showed that oxidation of As(III) to As(V) was enhanced by heterogeneous oxidation on kaolinite and illite surfaces.

Introduction

The occurrence of elevated levels of As in soils and groundwaters can compromise soil and water quality. Arsenic is ubiquitous in the earth's crust and is highest in marine shale materials, magmatic sulfides, and iron ores where As occurs as arsenopyrite (FeAsS), realgar (AsS), and orpiment (As_2S_3) (*1, 2*). Oxidative weathering and dissolution of As-containing minerals form dissolved inorganic As(III) and As(V) that are transported in surface or groundwaters and can become adsorbed on soil and sediment particles. Though the As concentration of uncontaminated soil is normally less than 6 mg kg^{-1} (*3*), anthropogenic sources of As such as arsenical pesticides (*4*), fertilizers (*5*), mine drainage (*6*), smelter wastes (*7*), and agricultural drainage water from certain arid regions (*8*) can elevate the levels of As in soil and water.

The distribution between dissolved As(III) and As(V) is dependent on redox potential (*9*). Under oxidizing conditions, the predominant species is As(V), which exists as deprotonated oxyanions of arsenic acid ($H_2AsO_4^-$, $HAsO_4^{2-}$, and AsO_4^{3-}) (*10*). Under mildly reducing conditions (>+100 mV), As(III) is thermodynamically stable (*10−12*) and exists as arsenious acid ($H_3AsO_3^0$, $H_2AsO_3^-$, and $HAsO_3^{2-}$). Recently, it has been recognized that As(III) is more prevalent in groundwater than was previously understood (*13*), which is of concern because it is more toxic than As(V) (*14*). In addition, As(III) is a neutral, uncharged molecule ($H_3AsO_3^0$, $pK_a = 9.2$) (*13*) at the pH of most natural waters and is more mobile because it is less strongly adsorbed on most mineral surfaces than the negatively charged As(V) oxyanions (*15*).

Previous studies of As adsorption on soil minerals have focused primarily on iron(III) oxides because of their high affinity for As(V). Investigations using extended X-ray absorption fine structure (EXAFS) (*16*), energy dispersive analysis of X-rays (EDAX) (*17*), and infrared (IR) spectroscopy (*18, 19*) have shown that As(V) forms high affinity, inner-sphere Fe-As(V) surface complexes. Recent work by Sun and Doner (*20*) using Fourier transform IR has shown that As(III) forms inner-sphere surface complexes similar to As(V) on goethite (α-FeOOH) surfaces. Decreases in the point of zero charge (PZC) of amorphous iron(III) oxide after reaction with As(III) also suggested that As(III) is specifically adsorbed on iron(III) oxide surfaces (*21*).

Only a few studies have investigated the adsorption of As(III) on aluminum oxides or aluminosilicate minerals despite the abundance of these materials in the terrestrial environment. One reason is the relatively weak affinity of aluminum oxides for As(III) when compared with iron(III) oxides. For example, Sakata (*22*) studied Japanese soils and found a high positive correlation between As(III) adsorption and dithionite-extractable Fe whereas As(III) adsorption was negatively correlated with oxalate-extractable Al. Activated alumina has a 2-fold higher affinity for As(V) than As(III) at pH 7 (*23*), and negligible removal of As(III) from drinking water was achieved by coagulation with alum ($Al_2(SO_4)_3$) (*24*). Kaolinite and montmorillonite were investigated as sorbents of As(III) and As(V) from landfill leachate and exhibited higher affinities for As(V) than As(III) (*25*). Though phyllosilicates exhibit a lower affinity for anions than iron and aluminum oxides, they can be abundant mineral components in soil and sediment.

The heterogeneous oxidation of adsorbed As(III) to As(V) on mineral surface is an important factor in controlling the overall mobility of As because of the differences in the adsorption behavior of As(III) and As(V). Synthetic birnessite (δ-MnO_2) oxidizes As(III) to As(V) with a release of soluble Mn(II) (*26*). The abiotic oxidation of As(III) by MnO_2 was also observed in freshwater lake sediments (*27*). Arsenic(III) oxidation did not occur in the presence of synthetic goethite (α-FeOOH) (*28*), short-range order iron(III) oxyhydroxide (*27*), or naturally occurring carbonate and silicate minerals (*29*).

Given the need for more detailed information about the reactions of As(III) with common minerals, the objectives of this work were several-fold: (1) to investigate the pH and ionic strength dependence of As(III) adsorption on reference clay minerals; (2) to compare As(III) and As(V) adsorption under identical experimental conditions; (3) to investigate the stability of As(III) adsorbed on clay mineral surfaces; and (4) to describe As(III) and As(V) adsorption envelopes (adsorption vs pH) using surface complexation modeling.

Materials and Methods

Mineral Sorbents. The phyllosilicate clay minerals used in this study were obtained from the Clay Minerals Society Source Clay Repository (Department of Geology, University of Missouri, Columbia, MO). Samples of sodium montmorillonite (SWy-1) from Crook County, WY, and kaolinite (KGa-1) from Washington County, GA, were used without further preparation. Illite (IMt-2) fragments from Silver Hill, MT, were ground with a mortar and pestle to pass a <500 μm

* Corresponding author phone: (909) 369-4884; fax: (909) 342-4962; e-mail: bmanning@ussl.ars.usda.gov.

S0013-936X(96)00810-3

sieve. Characterization of the clays by X-ray diffraction (XRD) analyses of both random powder mounts and oriented slide mounts indicated that KGa-1 contained traces of feldspar and vermiculite. Montmorillonite showed a trace impurity of mica, and illite was XRD pure. Specific surface areas of the clay sorbents were determined by single-point Brunauer–Emmett–Teller (BET) N_2 adsorption with a Quantisorb Jr. surface area analyzer (Quantachrome Corp., Syosset, NY) (see Table 3).

Amorphous $Al(OH)_3$ was prepared by a modification of a previous method (*30*) by mixing 300 mL of 1.5 M $AlCl_3$ with 800 mL of 4.0 M NaOH and shaking for 15 min (final pH 4.3). The precipitate suspension was transferred to 250-mL centrifuge bottles and centrifuged (10000*g*) for 20 min, and the supernatant was decanted. The solids were then air-dried and crushed with a mortar and pestle to pass a <500-μm sieve. The sample was found to be amorphous by XRD analysis, though undetectable short-range order was probably present in the material.

Arsenic Determination. Arsenic was determined in all extracts by high-performance liquid chromatography–hydride generation atomic absorption spectrophotometry (HPLC–HGAAS) as outlined in detail in a previous paper (*31*). A Dionex AS11 anion exchange column was coupled with continuous HGAAS detection allowing direct, simultaneous determination of As(III) and As(V) at concentrations down to 0.013 μM As. Most samples were also run by continuous flow-through HGAAS without HPLC separation for comparison, and excellent agreement between the two techniques was found for both single ion and mixed ion solutions. Arsenic single ion and mixed ion (As(III) + As(V)) working standards (0.07–0.4 μM As) were prepared fresh daily in either 0.005 M NaCl or 0.001 M PO_4 matrix for HPLC–HGAAS analysis.

As(III) and As(V) Adsorption Experiments. Stock solutions of 1000 mg L^{-1} As(III) or As(V) in deionized (DI) water were made from $NaAsO_2$ (Sigma) or $Na_2HAsO_4 \cdot 7H_2O$ (Sigma), respectively. Batch adsorption of As(III) and As(V) was examined by shaking clay suspensions in 40-mL polycarbonate centrifuge tubes containing 500 mg of clay in 20 mL of 0.4 μM As(III) or As(V) for 16 h. Experiments with am-$Al(OH)_3$ suspensions contained 50 mg of solid in 20 mL of 0.4 μM As(III). Suspension pH was adjusted with 0.1 M NaOH/HCl (KGa-1 and IMt-2) or 1.0 M NaOH/HCl (SWy-1 and am-$Al(OH)_3$) after addition of the 0.4 μM As(III) or As(V) solutions. Initial pH values before adjustment were approximately 4.5 (KGa-1 and am-$Al(OH)_3$) and 8.2 (SWy-1 and IMt-2). Ionic strength (*I*) was maintained using 0.005, 0.05, or 0.1 M NaCl background electrolyte. For am-$Al(OH)_3$ and SWy-1, however, the lowest *I* values possible, which also permitted varying suspension pH, were 0.02 and 0.015 M, respectively. After the 16-h reaction period, the tubes were centrifuged at 14400*g* for 10 min, and pH was determined directly in supernatants with an Orion glass combination pH electrode followed by filtering with 0.1 μm Whatman cellulose nitrate membranes. Arsenic speciation was then determined on these solutions. The fractional As(III) adsorption (%As(III) adsorbed) was calculated as

$$\%\ \text{As(III) adsorbed} = 100 \times \frac{([\text{As(III)}]_0 - [\text{As(T)}]_{\text{eqm}})}{[\text{As(III)}]_0} \quad (1)$$

where $[As(III)]_0$ is the initial As(III) added (0.4 μM As(III)) and $[As(T)]_{eqm}$ is the total equilibrium supernatant As concentration (As(III) + As(V)) after reaction with the solids.

Desorption of As(III) and As(V). The As(III)- and As(V)-treated clay solids were resuspended in 20 mL of 1 mM PO_4 buffer (50:50 KH_2PO_4:K_2HPO_4, pH 7). The purpose of this extraction was to desorb As(III) and As(V), which were associated with the solid phase by competitive ligand exchange with $H_2PO_4^-$ and HPO_4^{2-} anions that have similar adsorption behavior to As(V). The 1 mM PO_4/clay suspensions were shaken for 3 h followed by centrifugation (14400*g*) and filtration (0.1 μm). All samples were analyzed for As(III) and As(V) immediately and were not stored before analysis.

TABLE 1. Surface Reactions for As(III) and As(V) Adsorption on Clay Minerals Included in Constant Capacitance Model

	eq no.
Surface Acid–Base Reactions	
$SOH^a + H^+ \leftrightarrows SOH_2^+$	(1)
$SOH \leftrightarrows SO^- + H^+$	(2)
Mononuclear As(V) Adsorption	
$SOH + H_3AsO_4 \leftrightarrows SH_2AsO_4 + H_2O$	(3)
$SOH + H_3AsO_4 \leftrightarrows SHAsO_4^- + H_2O + H^+$	(4)
$SOH + H_3AsO_4 \leftrightarrows SAsO_4^{2-} + H_2O + 2H^+$	(5)
Mononuclear As(III) Adsorption	
$SOH + H_3AsO_3 \leftrightarrows SH_2AsO_3 + H_2O$	(6)
$SOH + H_3AsO_3 \leftrightarrows SHAsO_3^- + H_2O + H^+$	(7)
$SOH + H_3AsO_3 \leftrightarrows SAsO_3^{2-} + H_2O + 2H^+$	(8)
Binuclear As(V) Adsorption	
$2SOH + H_3AsO_4 \leftrightarrows S_2HAsO_4 + 2H_2O$	(9)
$2SOH + H_3AsO_4 \leftrightarrows S_2AsO_4^- + 2H_2O + H^+$	(10)
Binuclear As(III) Adsorption	
$2SOH + H_3AsO_3 \leftrightarrows S_2HAsO_3 + 2H_2O$	(11)
$2SOH + H_3AsO_3 \leftrightarrows S_2AsO_3^- + 2H_2O + H^+$	(12)

[a] *S*OH represents one reactive surface hydroxyl group bound to a surface metal ion *S*.

Effects of pH on As(III) Stability. The effect of solution pH on the stability of As(III) was investigated using a Mettler DL70 programmable autotitrator. The purpose was to determine the effects of solution pH on the homogeneous oxidation of As(III) to As(V). The titrator was programmed to maintain 60-mL volumes of 0.4 μM As(III) in 0.005 M NaCl at pH 4, 6, 8, 9, and 10 (three replicates at each pH) for a total of 72 h using 0.01 M NaOH or HCl titrant. The initial pH of the 0.4 μM As(III) solution was 5.1 ± 0.2, and the total volumes of titrant added to maintain the designated pH values for 72 h were approximately 1.7, 4.5, 8.5, and 11 mL of 0.01 M NaOH for pH 6, 8, 9, and 10, respectively. After 72 h, the speciation of As(III) and As(V) in the solutions was determined by HPLC–HGAAS.

Modeling As(III) and As(V) Adsorption Data. The constant capacitance model (CCM) (*32*) was used to describe As(III) and As(V) adsorption reactions on clay minerals as a function of pH for experiments where $I = 0.1$ M (as NaCl). The CCM is an equilibrium surface complexation model that assumes ion adsorption occurs by an inner-sphere ligand exchange mechanism. Detailed reviews of the theory and use of surface complexation models to describe ion adsorption on metal oxides are described elsewhere (*33*, *34*).

The computer program FITEQL 3.1 (*35*) was used to optimize As(III) and As(V) intrinsic surface complexation constants for the reactions given in Table 1. The generalized intrinsic surface complexation constant for a surface reaction (K_{rxn}(int)) is defined as the equilibrium constant for the reaction (K_{rxn}) multiplied by an exponential term, which accounts for the surface charge produced in the reaction

$$K_{\text{rxn}}(\text{int}) = K_{\text{rxn}} \exp(\pm nF\Psi_o/RT) \quad (2)$$

where *n* is the stoichiometric coefficient, *F* is the Faraday (9.65×10^{-4} C mol^{-1}), Ψ_o is the surface potential (V), *R* is the gas constant, and *T* is the temperature (*K*). The K_{rxn}(int) values used in modeling (e.g., $K_{SAs(III)}$(int) and $K_{SAs(V)}$(int)) are described in Table 2 and correspond to the surface reactions given in Table 1. The FITEQL program iteratively optimizes a set of *K*(int) by minimizing the differences between calculated and experimental adsorption data using a nonlinear least squares optimization routine. The goodness-of-fit parameter (V_Y) in FITEQL is defined as the overall variance

TABLE 2. Equilibrium Expressions for Intrinsic Surface Complexation Constants Used To Describe As(III) and As(V) Adsorption on Clay Minerals in FITEQL

	eq no.
Surface Acid−Base Reactions	
$K_{S+}(\text{int}) = [SOH_2^+][SOH]^{-1}[H^+]^{-1}\exp(F\Psi_o/RT)$[a]	(13)
$K_{S-}(\text{int}) = [SO^-][H^+][SOH]^{-1}\exp(-F\Psi_o/RT)$	(14)
Mononuclear As(V) Adsorption	
$K^1_{SAs(V)}(\text{int}) = [SH_2AsO_4][SOH]^{-1}[H_3AsO_4]^{-1}$	(15)
$K^2_{SAs(V)}(\text{int}) = [SHAsO_4^-][H^+][SOH]^{-1}[H_3AsO_4]^{-1}\exp(-F\Psi_o/RT)$	(16)
$K^3_{SAs(V)}(\text{int}) = [SAsO_4^{2-}][H^+]^2[SOH]^{-1}[H_3AsO_4]^{-1}\exp(-2F\Psi_o/RT)$	(17)
Mononuclear As(III) Adsorption	
$K^1_{SAs(III)}(\text{int}) = [SH_2AsO_3][SOH]^{-1}[H_3AsO_3]^{-1}$	(18)
$K^2_{SAs(III)}(\text{int}) = [SHAsO_3^-][H^+][SOH]^{-1}[H_3AsO_3]^{-1}\exp(-F\Psi_o/RT)$	(19)
$K^3_{SAs(III)}(\text{int}) = [SAsO_3^{2-}][H^+]^2[SOH]^{-1}[H_3AsO_3]^{-1}\exp(-2F\Psi_o/RT)$	(20)
Binuclear As(V) Adsorption	
$K^1_{S2As(V)}(\text{int}) = [S_2HAsO_4][SOH]^{-2}[H_3AsO_4]^{-1}$	(21)
$K^2_{S2As(V)}(\text{int}) = [S_2AsO_4^-][H^+][SOH]^{-2}[H_3AsO_4]^{-1}\exp(-F\Psi_o/RT)$	(22)
Binuclear As(III) Adsorption	
$K^1_{S2As(III)}(\text{int}) = [S_2HAsO_3][SOH]^{-2}[H_3AsO_3]^{-1}$	(23)
$K^2_{S2As(III)}(\text{int}) = [S_2AsO_3^-][H^+][SOH]^{-2}[H_3AsO_3]^{-1}\exp(-F\Psi_o/RT)$	(24)

[a] *S*OH represents one reactive surface hydroxyl group bound to a surface metal ion *S*.

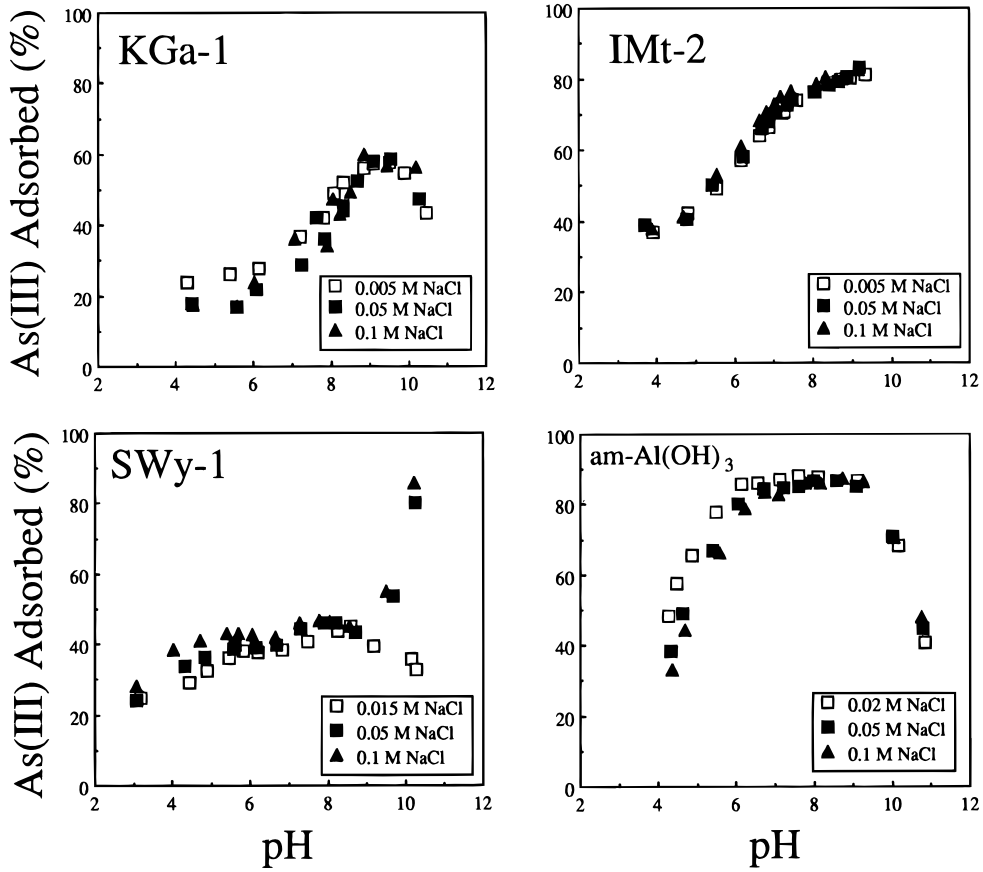

FIGURE 1. Effects of pH and ionic strength on the adsorption of As(III) on kaolinite (KGa-1), illite (IMt-2), montmorillonite (SWy-1), and amorphous aluminum hydroxide (am-Al(OH)$_3$). Reaction conditions: 25 g L^{-1} (KGa-1, SWy-1, and IMt-2) and 2.5 g L^{-1} (am-Al(OH)$_3$), [As(III)]$_0$ = 0.4 μM, reaction time = 16 h.

in Y

$$V_Y = \frac{\sum(Y_i/s_i)^2}{(n_p n_c) - n_a} \quad (3)$$

where Y_i is the residual for each adsorption data point i, s_i is the error estimate, n_p is the number of data points in the adsorption envelope, n_c is the number of system components for which both the total and free concentrations are known, and n_a is the number of adjustable parameters in the system (*35*).

Recently, EXAFS spectroscopy has provided evidence for the formation of inner-sphere, binuclear bridging complexes of oxyanions on hydrous ferric oxide surfaces (*16*, *36*). For this reason, two different bonding scenarios were used in describing As adsorption with the CCM by combining equations from Table 1. Monodentate mononuclear adsorption of As(V) was described by eqs 3−5 (Table 1), and for

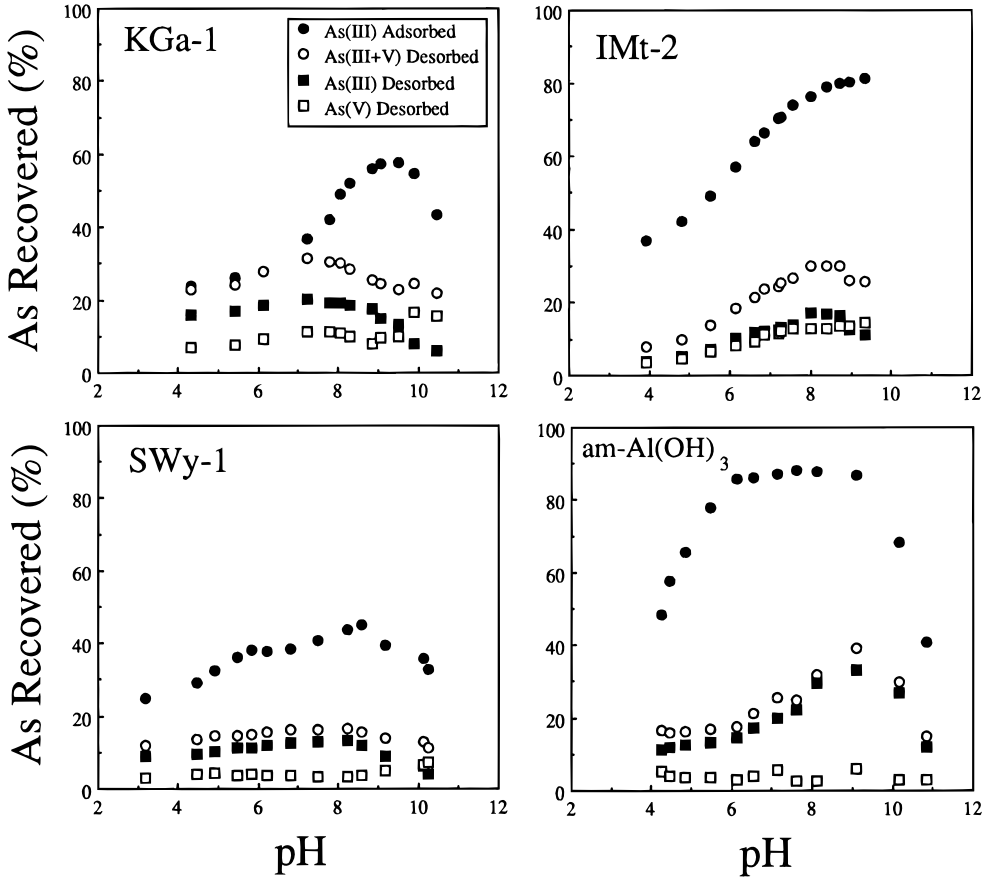

FIGURE 2. Recovery of As(III) and As(V) in 1 mM PO_4 extracts of As(III)-treated kaolinite (KGa-1), illite (IMt-2), montmorillonite (SWy-1), and amorphous aluminum hydroxide (am-Al$(OH)_3$). The % As recovered refers to percent of total As initially added to the system ($[As(III)]_0 = 0.4\ \mu M$). Reaction conditions: 25 g L^{-1} (KGa-1, SWy-1, and IMt-2) and 2.5 g L^{-1} (am-Al$(OH)_3$), reaction time = 3 h. The amount of As(III) initially adsorbed is also shown for comparison.

As(III), eqs 6−8 (Table 1) were used. A mixture of binuclear bridging plus monodentate mononuclear adsorption of As(V) (multinuclear adsorption) was described by eqs 5, 9, and 10 (Table 1). Multinuclear adsorption of As(III) was described by combining eqs 8, 11, and 12 (Table 1).

In all modeling cases, five adjustable parameters were optimized to achieve satisfactory fits of the CCM to the experimental data. This included three surface complexation constants plus two surface protonation constants (e.g., reactions 1−5, Table 1). However, FITEQL would not converge when the five adjustable parameters were optimized simultaneously. Therefore, a sequential optimization scheme was used where K_{S+}(int) and K_{S-}(int) starting values from previous work (*37*) were optimized first, followed by a separate optimization of the three As surface complexation constants while holding K_{S+}(int) and K_{S-}(int) as fixed values. This approach yielded the best fits of the model to experimental data based on values of V_Y in FITEQL. The final K_{S+}(int) and K_{S-}(int) values were self-consistent between As(III) and As(V) data sets for a given mineral.

Results and Discussion

As(III) Adsorption. The effects of both solution pH and *I* on the adsorption of As(III) on the four materials are shown in Figure 1. In general, minor ionic strength effects are observed, except for SWy-1, where the combination of high pH and high *I* resulted in increased As(III) removal from solution. Ionic strength had the least effect on As(III) binding to IMt-2. However, between pH 4 and pH 9, differences between As(III) adsorption on the other materials due to variations in *I* were typically less than 10%. Adsorption behavior that is unaffected by changes in *I* is macroscopic evidence for inner-sphere complexation (*38*, *39*). General similarities between the four materials include low As(III) adsorption at low pH and maximum As(III) adsorption between pH 7.5 and pH 9.5 (Figure 1). The pH 9.5 value coincides with the point of zero charge (PZC) of am-Al$(OH)_3$ particles (PZC = 9.5) and is slightly above the first $H_3AsO_3^0$ pK_a of 9.2. The am-Al$(OH)_3$ adsorbed a maximum of 0.142 μmol g^{-1} As(III) at pH 8 whereas the maximum As(III) adsorption by the phyllosilicates was 0.128 μmol g^{-1} As(III) (IMt-2, pH 9). This suggests that SiO_4 tetrahedra, which are major surface components of phyllosilicates, are less reactive than ≡Al-OH functional groups toward As(III).

The ideal unit formulas for kaolinitic minerals such as KGa-1 have Si/Al ratios of 1, whereas illitic minerals such as IMt-2 and smectites such as SWy-1 have Si/Al ratios of 2. Based on the greater reactivity of am-Al$(OH)_3$ toward As(III) than phyllosilicates, it would be expected that kaolinite, which contains exposed sheets of Al octahedra, would result in greater As(III) adsorption on KGa-1 than IMt-2. However IMt-2, which contains ≡Al-OH functional groups only at particle edge sites, adsorbs more As(III) than KGa-1. This may be due in part to the higher surface area of IMt-2. The PZC values for the phyllosilicates are typically below pH 3 due to permanent structural negative charge, and thus the net charge on these particles is negative at typical environmental pH values. Differences in the PZC values of the edge ≡Al-OH functional groups may affect As adsorption behavior, though these values are difficult to obtain experimentally.

Stability of As(III) in Clay-Water Suspensions. Desorption of adsorbed As from As(III)-treated solids with 1 mM PO_4 revealed that As(III) oxidation resulted in measurable surface-bound As(V) (Figure 2). The magnitude of As(V) recovery was dependent on the original suspension pH and the mineral. The solid samples extracted with 1 mM PO_4 were those that

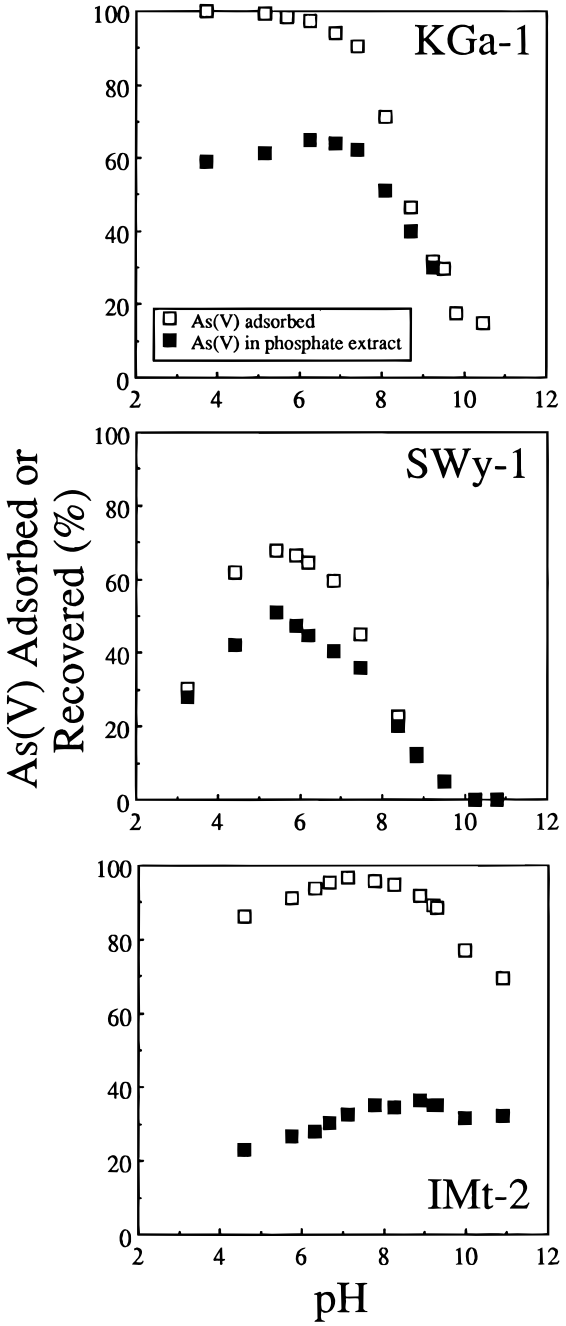

FIGURE 3. Adsorption and recoveries of As(V) from As(V)-treated clay minerals. Adsorption reaction conditions: 25 g L^{-1}, $[As(V)]_0$ = 0.4 μM, I = 0.1 M NaCl, reaction time = 16 h. Desorption reaction conditions: suspension density = 25 g L^{-1}, 1 mM PO_4 extraction solution, reaction time = 3 h.

had been equilibrated with As(III) at low I, though analysis of selected high I samples indicated that As(III) oxidation in clay suspensions did not depend on ionic strength (data not shown). Substantial As(V) was recovered in 1 mM PO_4 extracts of As(III)-treated KGa-1 and IMt-2 and was greatest at high pH.

Desorption of As(V) from As(V)-treated layer silicates with 1 mM PO_4 indicated that a portion of bound As(V) was not extractable (Figure 3). For example, the As(V) extraction efficiency for KGa-1, SWy-1, and IMt-2 at pH 7 was approximately 66, 80, and 33%, respectively. The As(V) extractability from KGa-1 and SWy-1 was nearly 100% above pH 8.5, but remained less than 50% for IMt-2. These data suggested that at most 50% of As(V) formed from As(III) oxidation in IMt-2 suspensions was exchangeable with $H_2PO_4^-$ and HPO_4^{2-} anions, whereas As(V) was probably completely recovered above pH 8.5 from KGa-1 and SWy-1.

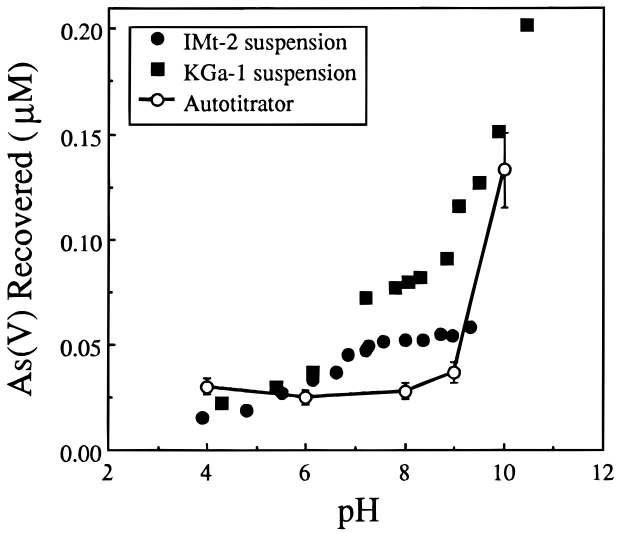

FIGURE 4. Formation of As(V) as affected by pH in As(III)-clay suspensions (KGa-1 and IMt-2) and in autotitrator experimental solutions. Suspension conditions: 25 g L^{-1} clay, $[As(III)]_0$ = 0.4 μM, reaction time = 16 h. Autotitrator experimental conditions: $[As(III)]_0$ = 0.4 μM, I = 0.005 M NaCl, titration time = 72 h.

The homogeneous oxidation of As(III) to As(V) in 0.4 μM As(III) solutions without clay solids at pH 4, 6, 8, 9, and 10 using the pH autotitrator indicated that substantial As(III) oxidation occurred at pH greater than 9 (Figure 4). After 72 h, autotitrator samples at pH 4, 6, and 8 contained less than 0.03 μM As(V). Total recovery of As(V) (suspension As(V) + PO_4-desorbed As(V)) in As(III)-KGa-1 and As(III)-IMt-2 clay suspensions was higher than in the autotitrator system. For example, at pH 8, the KGa-1 and IMt-2 clay mineral suspensions (25 g L^{-1}) produced 0.077 μM As(V) (19% of $[As(III)]_0$) and 0.052 μM As(V) (13% of $[As(III)]_0$), respectively. Recovery of As(V) in As(III)-KGa-1 suspensions increased with increasing pH (Figure 4) to a maximum at pH 10.4 forming 0.2 μM As(V) (50% of $[As(III)]_0$). These data suggest that both mineralogy and pH are critical factors in understanding the abiotic reactions of As(III).

We suspect that MnO_2 may have caused the partial oxidation of As(III) to As(V) in clay suspensions since this reaction has been confirmed in previous work (*26*−*29*). The MnO_2 content is low in the clay materials we studied (<0.006% w:w) (*40*, *41*). However, based on the reported As(III) oxidation by synthetic MnO_2 (*26*) and a calculation using an approximate As(III)/MnO_2 oxidation capacity of 0.12 mol of As(III):mole of MnO_2, the 25 g L^{-1} clay suspensions contain sufficient MnO_2 to cause the observed As(III) oxidation. The proposed sites of oxyanion adsorption on phyllosilicates are ≡Al-OH and ≡Al-OH_2^+ functional groups at exposed crystal edges (*42*−*44*). The fact that synthetic am-$Al(OH)_3$ is composed entirely of ≡Al-OH surface functional groups and the observation that very low levels of As(V) were recovered in the 1 mM PO_4 extracts of As(III)-treated am-$Al(OH)_3$ (Figure 2) suggest that ≡Al-OH in layer silicates are not contributing to the As(III) oxidation.

Modeling As(III) and As(V) Adsorption. The results of applying the CCM to As(III) and As(V) adsorption are indicated by lines in Figure 5. Model lines in Figure 5 are the sums of individual surface species. For example, mononuclear As(III) adsorption (solid lines) is $SH_2AsO_3^0$ + $SHAsO_3^-$ + $SAsO_3^{2-}$, and multinuclear As(III) adsorption (dotted lines) is $S_2HAsO_3^0$ + $S_2AsO_3^-$ + $SAsO_3^{2-}$. The As(III)/IMt-2 and As(III)/KGa-1 systems were complicated by pH-dependent oxidation of As(III) to As(V) (Figure 4). Therefore, modeling As(III) adsorption on KGa-1 and IMt-2 is most representative

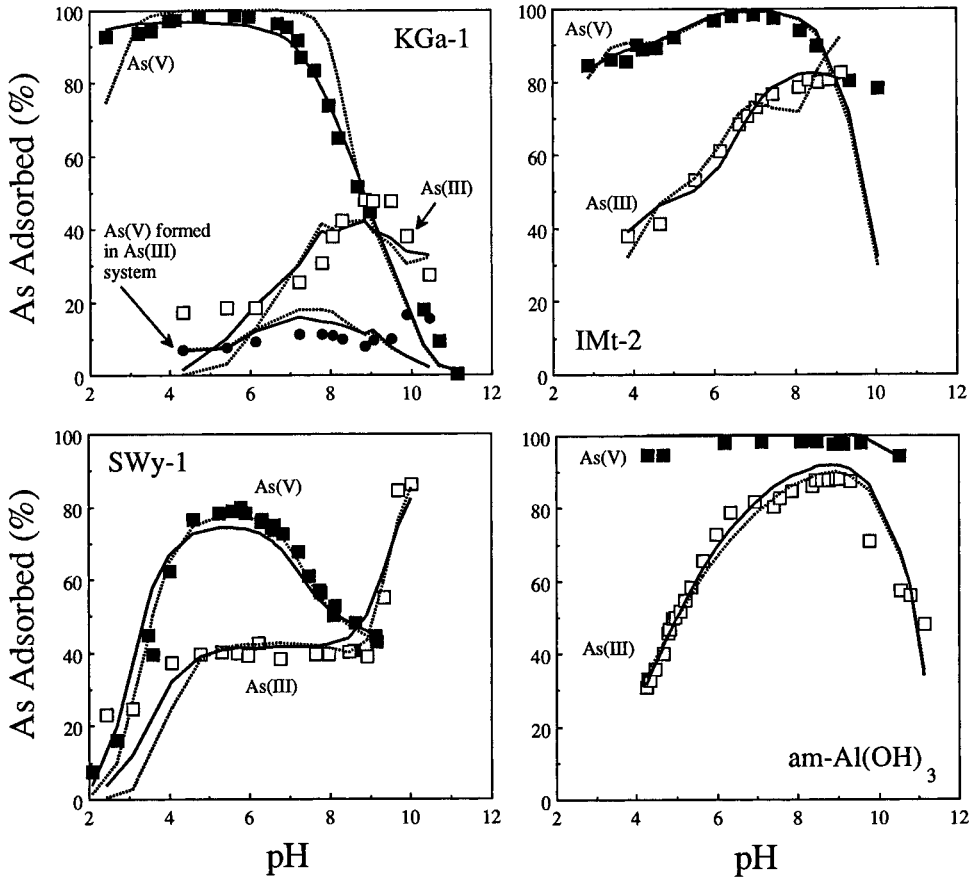

FIGURE 5. Adsorption of As(III) (□) and As(V) (■) on kaolinite (KGa-1), illite (IMt-2), montmorillonite (SWy-1), and amorphous aluminum hydroxide (am-Al(OH)$_3$) with constant capacitance model (CCM) outputs using the mononuclear (—) and multinuclear (···) assumptions. Reaction conditions: 25 g L^{-1} (KGa-1, SWy-1, and IMt-2) and 2.5 g L^{-1} (am-Al(OH)$_3$), [As(III)]$_0$ = 0.4 μM, I = 0.1 M NaCl, reaction time = 16 h.

TABLE 3. Numerical Input Values and Intrinsic Surface Complexation Constants for Mononuclear As(V) and As(III) Adsorption on Kaolinite (KGa-1), Montmorillonite (SWy-1), Illite (IMt-2), and Amorphous Al(OH)$_3$ Optimized in FITEQL Using Constant Capacitance Model

parameter	KGa-1	SWy-1	IMt-2	am-Al(OH)$_3$
BET surface area (m^2 g^{-1})	9.1	18.6	24.2	5.9 (45.0)[a]
suspension density (g L^{-1})	25	25	25	2.5
site density (mol L^{-1} ×10^{-5})	6.10	2.77	2.90	43.2
log K_{S+}(int)[b]	6.28	3.80	3.53	9.10
log K_{S-}(int)	−9.28	−10.2	−7.10	−10.5
log $K^1_{SAs(V)}$(int)	9.33	−1.63	6.50	NC[c]
log $K^2_{SAs(V)}$(int)	3.25	2.82	3.25	6.43
log $K^3_{SAs(V)}$(int)	−4.75	−4.69	−1.95	−3.89
$V_{SAs(V)}$[d]	0.018	0.035	0.66	0.007
log $K^1_{SAs(III)}$(int)	3.97	4.41	4.49	NC
log $K^2_{SAs(III)}$(int)	−3.66	−4.65	−1.85	−5.02
log $K^3_{SAs(III)}$(int)	−14.1	−13.7	−11.2	−15.0
$V_{SAs(III)}$	0.078	0.090	0.009	0.027

[a] Surface area optimized in FITEQL = 45 m^2 g^{-1}. [b] Intrinsic surface complexation constants were calculated as mol L^{-1}. [c] NC, no convergence. [d] $V_{SAs(V)}$ = FITEQL goodness of fit parameter for mononuclear As(V) complexation.

below pH 8 where As(III) oxidation was less than 12% of [As(III)]$_0$ for IMt-2 and 19% of [As(III)]$_0$ for KGa-1. To model the special case of the As(III)-KGa-1 system (where appreciable As(III) had oxidized to As(V)) we used the $K_{SAs(V)}$(int) values (mononuclear and multinuclear) that were optimized in the As(V)-KGa-1 system to predict adsorbed As(V) resulting from As(III) oxidation. This procedure was not performed on the other materials because either As(V) was not formed in large enough quantities (SWy-1 and am-Al(OH)$_3$) or poor recovery of As(V) made it difficult to verify the exact amount of As(V) formed in the system (IMt-2, see Figure 3).

In most cases, the constant capacitance model adequately described As(III) and As(V) adsorption envelopes on the materials over the pH range 4−9. The assumption of inner-sphere As(III) and As(V) adsorption at a single surface *S*OH functional group (mononuclear complexes) resulted in the set of intrinsic surface complexation constants given in Table 3. Mononuclear and multinuclear complex assumptions gave comparable fits of the CCM to experimental As(III) and As(V) adsorption data based on values of V_Y (Tables 3 and 4). However, the prevailing understanding of oxyanion surface complex formation on iron(III) oxides based on EXAFS spectra provides evidence for predominantly multinuclear complexes (*16*, *36*). Thus, information from EXAFS should be used as a constraint on assumptions used in surface complexation modeling, especially if evidence for multinuclear As(III) and

TABLE 4. Intrinsic Surface Complexation Constants for Multinuclear (Mononuclear + Binuclear) As(V) and As(III) Adsorption on Kaolinite (KGa-1), Montmorillonite (SWy-1), Illite (IMt-2), and Amorphous $Al(OH)_3$ Optimized in FITEQL Using Constant Capacitance Model[a]

parameter	KGa-1	SWy-1	IMt-2	am-$Al(OH)_3$
log $K^1_{S2As(V)}$(int)[b]	16.2	10.7	11.8	NC[c]
log $K^2_{S2As(V)}$(int)	NC	7.48	7.75	9.50
log $K^3_{SAs(V)}$(int)	−4.76	−4.72	−2.00	−3.51
$V_{S2As(V)}$[d]	0.081	0.015	0.700	0.007
log $K^1_{S2As(III)}$(int)	8.23	8.99	9.07	7.58
log $K^2_{S2As(III)}$(int)	−0.664	NC	3.00	−2.43
log $K^3_{SAs(III)}$(int)	−13.67	−13.6	−10.3	−14.8
$V_{S2As(III)}$	0.156	0.144	0.028	0.025

[a] See Table 1 for log K_+(int) and log K_-(int) values. [b] Intrinsic surface complexation constants were calculated as mol L^{-1}. [c] NC, no convergence. [d] $V_{S2As(V)}$ = FITEQL goodness of fit parameter for multinuclear As(V) complexation.

As(V) complexes on ≡Al-OH surface functional groups is obtained.

Our results indicate that As(III) is stable in solution between pH 4 and pH 9, but that homogeneous oxidation of As(III) to As(V) occurs in solutions at or above pH 9.2 (above the first pK_a of H_3AsO_3). Oxidation of As(III) to As(V) was also enhanced in the presence of KGa-1 and IMt-2 by heterogeneous reactions with components on these mineral surfaces. Because As(V) formation in am-$Al(OH)_3$ suspensions was low, we feel that the As(III) oxidation in KGa-1 and IMt-2 suspensions was caused by heterogeneous reactions with solid phase components other than ≡Al-OH edge sites. The As(III) oxidation process results in more strongly adsorbed As(V), which would cause a decrease in the mobility of As in the environment. Modeling As(III) adsorption on many common mineral surfaces may not always be valid because of the potential for long-term heterogeneous oxidation of adsorbed As(III) and homogeneous oxidation of dissolved As(III) at alkaline pH. Our work suggests that long-term, field-scale modeling of As mobility in soils and aquifers must consider the effects of pH and mineralogy, which will influence both adsorption and abiotic oxidation of As(III).

Literature Cited

(1) Tanaka, T. *Appl. Organomet. Chem.* **1988**, *2*, 283−295.
(2) Huang, Y.-C. In *Arsenic in the environment, part I: Cycling and characterization*; Nriagu, J. O., Ed.; Wiley-Interscience: New York, 1988.
(3) Bowen, H. J. M. *Elemental Chemistry of the Elements*; Academic Press: London and New York, 1979.
(4) Mariner, P. E.; Holzmer, F. J.; Jackson, R. E.; Meinardus, H. W. *Environ Sci. Technol.* **1996**, *30*, 1645−1651.
(5) Landrigan, P. *Am. J. Ind. Med.* **1981**, *2*, 5−14.
(6) Johnson, C. A.; Thornton, I. *Water Res.* **1987**, *21*, 359.
(7) Davis, A.; Ruby, M. V.; Bloom, M.; Schoof, R.; Freeman, G.; Bergstrom, P. D. *Environ. Sci. Technol.* **1996**, *30*, 392−399.
(8) Fujii, R.; Swain, W. C. Areal distribution of selected trace elements, salinity, and major ions in shallow ground water, Tulare Basin, southern San Joaquin Valley. *Water Resour. Invest. (U.S. Geol. Surv.)* **1995**, *No. 95-4048*.
(9) Cherry, J. A.; Shaikh, A. U.; Tallman, D. E.; Nicholson, R. V. *J. Hydrol.* **1979**, *43*, 373−392.
(10) Sadiq, M.; Zaida, T. H.; Mian, A. A. *Water Air Soil Pollut.* **1983**, *20*, 369−377.
(11) Masscheleyn, P. H.; Delaune, R. D.; Patrick, W. H., Jr. *J. Environ. Qual.* **1991**, *20*, 522−527.
(12) Ferguson, J. F.; Gavis, J. *Water. Res.* **1972**, *6*, 1259−1274.
(13) Korte, N. E.; Fernando, Q. *Crit. Rev. Environ. Control* **1991**, *21*, 1−39.
(14) Knowles, F. C.; Benson, A. A. *Trends Biochem. Sci.* **1983**, *8*, 178−180.
(15) Gulens, J.; Champ, D. R.; Jackson, R. E. In *Chemistry of Water Supply Treatment and Distribution*; Rubia, A. J., Ed.; Ann Arbor Science Publishers: Ann Arbor, MI, 1973.
(16) Waychunas, G. A.; Rea, B. A.; Fuller, C. C.; Davis, J. A. *Geochim. Cosmochim. Acta* **1993**, *57*, 2251−2269.
(17) Hsia, T. H.; Lo, S. L.; Lin, C. F.; Lee, D. Y. *Colloids Surf. A: Physicochem. Eng. Aspects* **1994**, *85*, 1−7.
(18) Lumsdon, D. G.; Fraser, A. R.; Russell, J. D.; Livesey, N. T. *J. Soil Sci.* **1994**, *35*, 381−386.
(19) Harrison, J. B.; Berkheiser, V. E. *Clays Clay Miner.* **1982**, *30*, 97−102.
(20) Sun, X.; Doner, H. E. *Soil Sci.* **1996**, *161*, 865−872.
(21) Pierce, M. L.; Moore, C. B. *Water Res.* **1982**, *16*, 1247−1253.
(22) Sakata, M. *Environ Sci. Technol.* **1987**, *21*, 1126−1130.
(23) Ghosh, M. M.; Yuan, J. R. *Environ. Prog.* **1987**, *6*, 150−157.
(24) Hering, J. G.; Chen, P.-Y.; Wilkie, J. A.; Elimelech, M. L. *J. Environ. Eng., ASCE* In press.
(25) Frost, R. R.; Griffin, R. A. *Soil Sci. Soc. Am. J.* **1977**, *41*, 53−57.
(26) Scott, M. J.; Morgan, J. J. *Environ. Sci. Technol.* **1995**, *29*, 1898−1905.
(27) Oscarson, D. W.; Huang, P. M.; Liaw, W. K. *J. Environ. Qual.* **1980**, *9*, 700−703.
(28) Scott, M. J. Ph.D. Thesis, California Institute of Technology, Pasadena, CA, 1991.
(29) Oscarson, D. W.; Huang, P. M.; Liaw, W. K. *Clays Clay Miner.* **1981**, *29*, 219−225.
(30) Sims, J. R.; Bingham, F. T. *Soil Sci. Soc. Am. Proc.* **1968**, *32*, 364−369.
(31) Manning, B. A.; Martens, D. A. *Environ. Sci. Technol.* **1997**, *31*, 171−177.
(32) Stumm, W.; Kummert, R.; Sigg, L. *Croat. Chem. Acta* **1980**, *53*, 291−312.
(33) Goldberg, S.; Davis, J. A.; Hem, J. D. In *The Environmental Chemistry of Aluminum*; Sposito, G., Ed.; CRC Lewis Publishers: Boca Raton, FL, 1996.
(34) Dzombak, D. A.; Morel, F. M. M. *Surface Complexation Modeling, Hydrous Ferric Oxide*; John Wiley & Sons: New York, 1990.
(35) Herbelin, A. L.; Westall, J. C. *FITEQL: A computer program for the determination of chemical equilibrium constants from experimental data*; Report 94-01, Oregon State University: Corvallis, OR, 1994.
(36) Manceau, A.; Charlet, L. *J. Colloid Interface Sci.* **1994**, *168*, 87−93.
(37) Manning, B. A.; Goldberg, S. *Clays Clay Miner.* **1996**, *44*, 609−623.
(38) Hayes, K. F.; Papelis, C.; Leckie, J. *J. Colloid Interface Sci.* **1988**, *125*, 717−726.
(39) Hingston, F. J.; Posner, A. M.; Quirk, J. P. *Adv. Chem. Ser.* **1968**, *79*, 82−90.
(40) van Olphen, H.; Fripiat, J. J. *Data Handbook for Clay Materials and Other Non-Metallic Minerals*; Pergamon: Oxford, 1979.
(41) Hower, J.; Mowatt, T. C. *Am. Mineral.* **1966**, *51*, 825−854.
(42) Keren, R.; Talpaz, H. *Soil Sci. Soc. Am. J.* **1984**, *48*, 555−559.
(43) Swartzen-Allen, L. S.; Matijevic, E. *Chem. Rev.* **1974**, *74*, 385−400.
(44) Muljadi, D.; Posner, A. M.; Quirk, J. P. *J. Soil Sci.* **1966**, *17*, 212−229.

Received for review September 20, 1996. Revised manuscript received March 3, 1997. Accepted March 7, 1997.[⊗]

ES9608104

[⊗] Abstract published in *Advance ACS Abstracts,* May 15, 1997.